High-Precision Positioning by Structural Design Using Vibration Node

Kenta Seki, Hiroaki Matsuura, Makoto Iwasaki, and Hiromu Hirai
Department of Computer Science & Engineering
Nagoya Institute of Technology
Gokiso, Showa, Nagoya, 4668555, Japan
Email: k-seki@nitech.ac.jp

***Abstract*—This paper presents a structural and controller design for fast and high-precision positioning systems. In order to achieve the high positioning performance, effects of mechanical vibration modes at around the control bandwidth on the performance should be compensated, where the vibration suppression is one of promising techniques from the viewpoints of the controller design as well as the optimization of mechanism. In this research, therefore, the primary vibration mode is canceled by the structural design considering node of the vibration modes, clarifying the guideline of structural design on the basis of a mode shape obtained by modal analyses. According to the designed mechanism, the controller for the fast and high-precision positioning can be easily designed by the simple structure. The proposed approach has been verified by experiments using a positioning device for industrial galvano scanners.**

I. Introduction

High-precision positioning is one of indispensable techniques in a wide variety of high performance mechatronic systems, such as data storage devices, machine tools, and industrial robots, from the viewpoints of high productivity, high quality of products, and total cost reduction [1]. In order to provide the precise positioning performance in mechatronic systems, the feedback controller should be designed under the consideration of both the expansion of servo bandwidth and system stability. However, since most of mechanisms inherently include vibration modes, the resonant vibration and/or the system instability due to the modes prevent the control bandwidth from being expanded when the control response frequency approaches the vibration natural frequency (primary vibration mode) [2][3]. Therefore, the control system should be designed by considering the influence of vibration modes in mechanism.

As one of typical approaches of the controller design, the gain compensation based on small gain theorem using notch filters has been widely applied to compensate for the effects of vibration modes. However, in the cases that the servo bandwidth approaches the primary resonant frequency, sufficient system stability cannot be achieved by influence of the phase delay due to the notch filter. As the other approach, although the sensor feedback using strain signal has been also proposed [4][5][6], the implementation of sensors is difficult from a viewpoint of sensor cost. Therefore, not only controller design but also structural design should be simultaneously taken into consideration to realize the high-precision positioning mechanisms.

This paper presents a structural and controller design approach to realize high-presicion positioning for galvano scanners including mechanical vibration modes [7][8]. In the structural design, the primary vibration mode is canceled by the structural design considering vibration node of the mode, where the guideline of structural design is clarified on the basis of a mode shape obtained by modal analyses. In the approach, a dynamic model of the plant is modeled by a lumped parameter model, and the vibration node can be determined by simple structure change on the basis of eigenvector analyzed by an eigenvalue problem. Since the displacement in the observation point becomes zero even if the vibration is excited, the vibration mode becomes uncontrollable and/or unobservable. In other words, from the viewpoint of a transfer function of the plant, pole-zero cancellation of the vibration mode can be achieved. According to the designed mechanism, the expansion of the servo bandwidth of the positioning system can be easily achieved by the changed structure. The effectiveness of the proposed approach has been verified by experiments using a positioning device for galvano scanners.

II. Positioning Mechanism and Frequency Characteristics

A. Configuration of positioning system

Figure 1 shows the structure of moving part of galvano scanner as a prototype. The moving part is composed of a mirror, a servo motor (rotor), and an angle sensor, where the shaft is supported by the bearings. Fig.2 shows a configuration of positioning device for the galvano scanner as an experimental setup [6][8]. The motor angle y is detected by a sensor and is transferred in a DSP (Digital Signal Processor) controller through an interface. The servo motor is driven by a current controlled amplifier with the control input u generated by the position controller (sampling time: $T_s = 20\mu s$).

B. Frequency characteristics of plant

The galvano scanner can be modeled by a multi-degrees of freedom vibration system whose frequency characteristics of the motor angle y for the control input u are plotted by solid lines in Fig.3 as an measurement result. From the figure, the mechanism mainly includes primary (4300Hz) and 2nd

978-1-4244-5226-2/10/$26.00 ©2010 IEEE

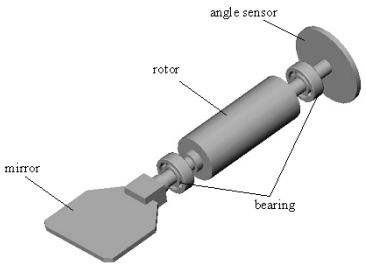

Fig. 1. Moving part of galvano scanner.

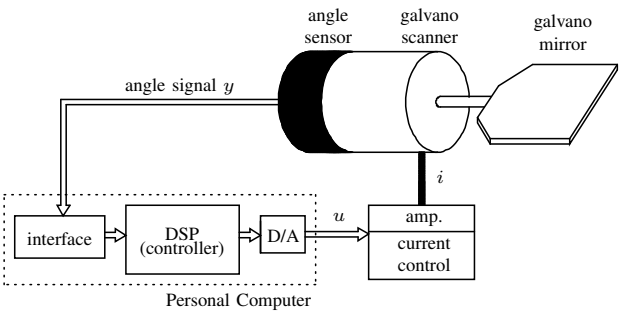

Fig. 2. Schematic configuration of experimental setup.

(6600Hz) vibration modes, affecting the positioning performance. By considering these vibration modes, the following polynomial is formulated as a plant model, consisting a rigid mode, vibration modes up to $n = 2$, and a dead time component:

$$P_1(s) = K_p \cdot e^{-Ls} \left(\frac{1}{s^2} + \sum_{n=1}^{2} \frac{a_n}{s^2 + 2\zeta_n \omega_n s + \omega_n^2} \right), \quad (1)$$

where K_p : gain includes moment of inertia, torque constant of motor and gain of current control system, ω_n : natural angular frequency of nth vibration mode, ζ_n : damping coefficient of nth vibration mode, a_n : modal constant of nth vibration mode, and L : equivalent dead time, respectively. The broken lines in Fig.3 show the frequency characteristic of the mathematical model $P_1(s)$, and Table I indicates the parameters of (1).

The desired control specification for the positioning system is given as a point-to-point positioning with the settling time of up to 0.8 ms for the typical positioning stroke of 1.5 mm. This settling time means the achievement of servo bandwidth about 1/3 frequency comparing to the primary vibration mode, requiring a fast and precise positioning performance with resonant vibration suppression, and improvement of sensitivity characteristic for the disturbances. However, since the primary vibration mode of this plant is antiphase vibration mode, it is generally difficult to control. Therefore, the servo bandwidth is expected to be limited unless the vibration mode is stabilized by the controller design.

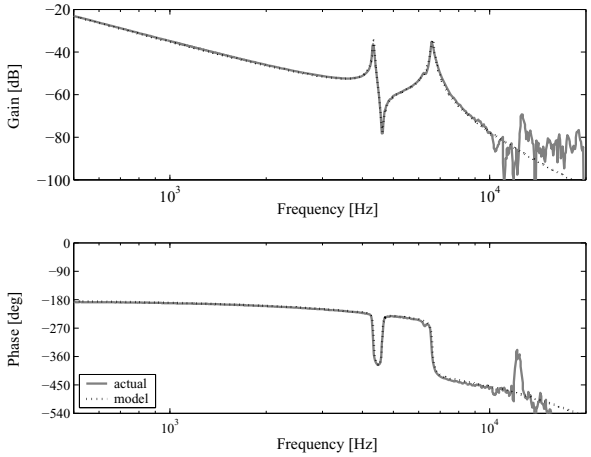

Fig. 3. Frequency characteristics of plant system.

TABLE I
PARAMETERS OF PLANT MODEL.

ω_1 [rad/s]	$2\pi\times$ 4340	ζ_1	0.005	a_1	-0.2
ω_2 [rad/s]	$2\pi\times$ 6630	ζ_2	0.009	a_2	-0.9
K_p	2.3×10^4	L [μs]	13.6		

III. STRUCTURAL DESIGN USING VIBRATION NODE

A. Modeling by lumped parameter

In this research, the vibration property of the galvano scanner is clarified by modal analyses before the controller design, where pole-zero cancellation of the mechanism is achieved by the structural design on the basis of the analyses. Moving part of the galvano scanner in Fig.1 is composed of three lumped inertia (mirror, rotor and sensor). In addition, the plant model in (1) is expressed by a rigid mode and two vibration modes. A dynamic model of the galvano scanner, therefore, can be modeled as three inertia lumped parameter of both free ends as shown in Fig.4. In the figure, J : lumped inertia, k : torsion spring, c : damper, θ : angular displacement of each inertia, and τ : torque, respectively. The torque is applied to the lumped inertia J_2 of rotor. The motion equation on the basis of Fig.4 can be expressed as follows:

$$[\boldsymbol{J}]\{\ddot{\theta}\} + [\boldsymbol{C}]\{\dot{\theta}\} + [\boldsymbol{K}]\{\theta\} = \{f\}, \quad (2)$$

where $[\boldsymbol{J}]$: inertia matrix, $[\boldsymbol{C}]$: damping matrix, $[\boldsymbol{K}]$: stiffness matrix, $\{\theta\}$: angular displacement vector, and $\{f\}$: force vector, respectively. These matrices and vectors are given as follows.

$$[\boldsymbol{J}] = \begin{bmatrix} J_1 & 0 & 0 \\ 0 & J_2 & 0 \\ 0 & 0 & J_3 \end{bmatrix} \quad (3)$$

$$[\boldsymbol{C}] = \begin{bmatrix} c_1 & -c_1 & 0 \\ -c_1 & c_1 + c_2 & -c_2 \\ 0 & -c_2 & c_2 \end{bmatrix} \quad (4)$$

$$[\boldsymbol{K}] = \begin{bmatrix} k_1 & -k_1 & 0 \\ -k_1 & k_1 + k_2 & -k_2 \\ 0 & -k_2 & k_2 \end{bmatrix} \quad (5)$$

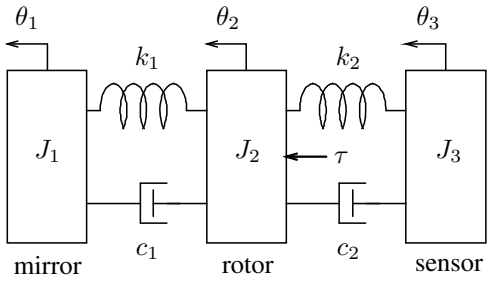

Fig. 4. Lumped parameter model of plant.

$$\{\theta\} = \begin{bmatrix} \theta_1 & \theta_2 & \theta_3 \end{bmatrix}^T \tag{6}$$

$$\{f\} = \begin{bmatrix} 0 & \tau & 0 \end{bmatrix}^T \tag{7}$$

B. Modal analyses

For the motion equation of (2), natural frequencies and shapes of vibration mode can be calculated by a solving generalized eigenvalue problem as an undamped free vibration system ($c = 0$, $f = 0$). By substituting damping matrix $[\boldsymbol{C}] = \mathbf{0}$ and force vector $\{f\} = \mathbf{0}$, (2) can be derived as follows.

$$[\boldsymbol{J}]\{\ddot{\theta}\} + [\boldsymbol{K}]\{\theta\} = \mathbf{0} \tag{8}$$

By substituting steady-state vibration $\theta = \theta e^{j\omega t}$ for (8) and dividing both sides by $e^{j\omega t}$, (8) can be given as follows.

$$\left(-\omega^2[\boldsymbol{J}] + [\boldsymbol{K}]\right)\{\theta\} = \mathbf{0} \tag{9}$$

Since the motion of the system satisfies $\{\theta\} \neq 0$, (9) can be modified as:

$$\left(-\omega^2[\boldsymbol{J}] + [\boldsymbol{K}]\right) = \mathbf{0}. \tag{10}$$

By combining the characteristic equations of (3), (5), and (10), the natural angular frequency can be calculated. Table II indicates the calculation result. Here, each inertia and stiffness are calculated by the materials, shapes, and dimensions of the moving part. ω_1 and ω_2 in Table II are comparatively corresponding to the identified parameters in Table I. By substituting natural angular frequencies in Table II into (9), the matrix composed of natural mode vectors is expressed as follows:

$$\begin{aligned}[\phi] &= \begin{bmatrix} \phi_{11} & \phi_{12} & \phi_{13} \\ \phi_{21} & \phi_{22} & \phi_{23} \\ \phi_{31} & \phi_{32} & \phi_{33} \end{bmatrix} \\ &= \begin{bmatrix} 1.0 & 1.0 & 1.0 \\ 1.0 & \frac{\alpha}{k_1} & \frac{\alpha}{k_1} \\ 1.0 & \frac{\alpha\times\beta - k_1^2}{k_1 k_2} & \frac{\alpha\times\beta - k_1^2}{k_1 k_2} \end{bmatrix} \\ &= \begin{bmatrix} 1.0 & 1.0 & 1.0 \\ 1.0 & 0.18 & -0.92 \\ 1.0 & -0.80 & 0.48 \end{bmatrix}, \end{aligned} \tag{11}$$

TABLE II
CALCULATION RESULT OF NATURAL ANGULAR FREQUENCIES.

ω_0 [rad/s]	ω_1 [rad/s]	ω_2 [rad/s]
0	$2\pi \times 4160$	$2\pi \times 6380$

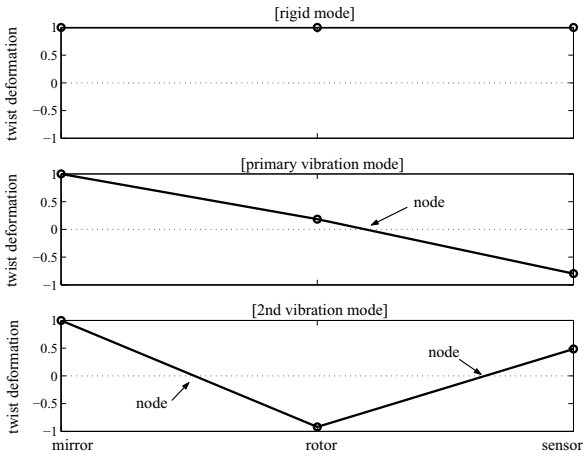

Fig. 5. Mode shapes for each vibration mode.

where,

$$\alpha = k_1 - \omega^2 J_1,$$
$$\beta = k_1 + k_2 - \omega^2 J_2.$$

Here, (11) is expressed in the amplitude ratio of the angular displacement θ_2 and θ_3 for θ_1. In (11), each column indicates the amplitude ratio corresponding to each natural angular frequency, while each row indicates the amplitude ratio of each inertia (1st row : the mirror, 2nd row : the rotor, and 3rd row : the sensor).

Figure 5 shows mode shapes for each vibration mode corresponding to the column of (11), where the upper figure indicates ω_0 in Table II (1st column of (11)), the middle figure indicates ω_1 in Table II (2nd column of (11)), and the bottom figure indicates ω_2 in Table II (3rd column of (11)), respectively. In the upper figure, since the whole amplitude ratio is 1.0 and $\omega_0 = 0$, it means rigid mode. In the primary vibration mode shown in the middle figure, one vibration node (the point of amplitude ratio = 0) exists between rotor and sensor. On the other hand, in the 2nd vibration mode shown in the bottom figure, two vibration nodes exist between mirror, rotor and sensor.

In the following section, the structure of galvano scanner is designed to achieve the vibration node in primary vibration mode based on the analytical result in this section.

C. Structural design and its result

Since the displacement at the vibration node becomes zero, the structure should be changed so that one element of 2nd row in (11) (mode vector of 2nd vibration mode) becomes zero. From the structure of galvano scanner shown in Fig.1, mirror and sensor inertia are located at both ends of the shaft.

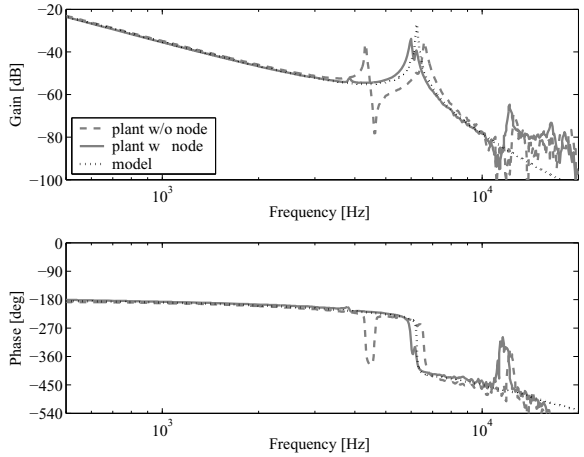

Fig. 6. Frequency characteristics of y for u.

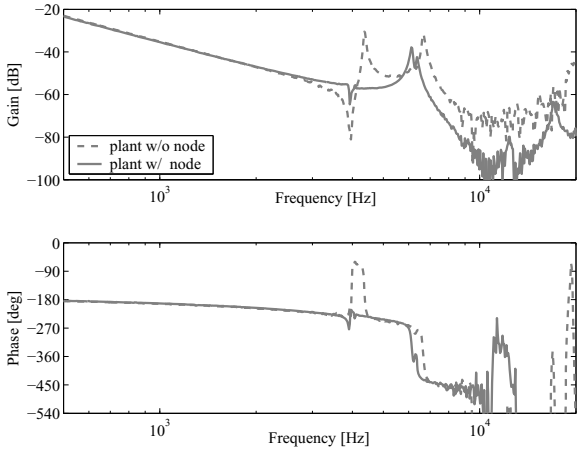

Fig. 7. Frequency characteristics of y_l for u.

In addition, from the Fig.5, the vibration node exists proximity of rotor inertia in the primary vibration mode. In this research, therefore, the part of rotor inertia is realized as a vibration node of primary vibration mode. It means that the primary vibration mode is uncontrollable as the mechanism because applying point of force becomes the vibration node.

In order to realize the vibration node for the rotor position in the primary vibration mode, ϕ_{22} of (11) should be zero. Therefore, the following equation should be satisfied.

$$\omega_1^2 J_1 = k_1 \tag{12}$$

The ratio of left side to right side in (12) for the galvano scanner is $1.0 : 1.2$. In order to satisfy (12), therefore, it is necessary to enlarge the mirror inertia J_1 or to reduce the torsion stiffness k_1 between mirror and rotor. For the fast positioning, since enlarging the inertia should be undesired, the torsion stiffness should be reduced in this case. The torsion stiffness k_1 is given as follows:

$$k_1 = \frac{GI_p}{\ell_1}, \tag{13}$$

where G : modulus of rigidity, I_p : polar moment of inertia area, ℓ_1 : length between mirror inertia and rotor inertia, respectively. Since the modulus of rigidity or the polar moment of inertia area is required by the modification of material or shape, the length between mirror and rotor is lengthened in this research. Here, the amount of length modification is several mm ($2 \sim 4$ % against the total length of shaft).

Frequency characteristics of plant after structural change by the above guideline are shown in Figs.6 and 7. Fig.6 indicates the frequency characteristics of sensor angle y for control input u, and Fig.7 indicates the frequency characteristics of mirror angle y_l for control input u. Here, mirror angle is detected by a position sensitive detector (PSD) using a semiconductor laser for detection use [8]. From Figs.6 and 7, since the applying point of force locates at the vibration node, the cancellation of the primary vibration mode can be realized for the observation point of both mirror and sensor. However, the natural angular frequency of the 2nd vibration mode decreases in lower value by reducing reduced the stiffness of structure. From the Fig.6, mathematical model is given as follows for (1).

$$P_2(s) = K_p \cdot e^{-Ls}\left(\frac{1}{s^2} + \frac{a_v}{s^2 + 2\zeta_v\omega_v s + \omega_v^2}\right), \tag{14}$$

The parameters of (14) list in Table III, while the frequency characteristic is indicated by the dotted lines in Fig.6.

TABLE III
PARAMETERS OF PLANT MODEL WITH VIBRATION NODE.

ω_v [rad/s]	$2\pi\times$ 6250	ζ_v	0.005	a_v	-1.1

IV. CONTROLLER DESIGN OF POSITIONING SYSTEM

A. Configuration of control system

Figure 8 indicates a block diagram of 2-degrees-of-freedom control structure based on the coprime factorization expression, where $P(s)$: plant, $N(z), D(z)$: feedforward compensators, $C(z)$: feedback compensator, $\mathcal{S}$: sampler, $\mathcal{H}$: hold, r : original position reference, and r^* : alternative position command trajectory, respectively. In the following section, compensators in the Fig.8 are designed for the plant without vibration node $P_1(s)$ (conventional) and the plant with vibration node $P_2(s)$ (proposed).

B. Design of feedback compensator

In order to ensure the sufficient stability margin of the control system including vibration modes and to expand the servo bandwidth, the feedback compensator $C(s)$ for each plant is designed as follows.

- for conventional plant $P_1(s)$

$$C_1(s) = K_1\frac{s+\omega_{a1}}{s}\frac{s+\omega_{c1}}{s+\omega_{b1}}\frac{s^2+2\zeta_a\omega_{nf}s+\omega_{nf}^2}{s^2+2\zeta_b\omega_{nf}s+\omega_{nf}^2} \tag{15}$$

- for proposed plant $P_2(s)$

$$C_2(s) = K_2\frac{s+\omega_{a2}}{s}\frac{s+\omega_{c2}}{s+\omega_{b2}} \tag{16}$$

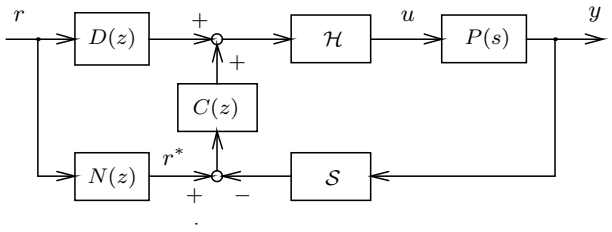

Fig. 8. Block diagram of positioning system.

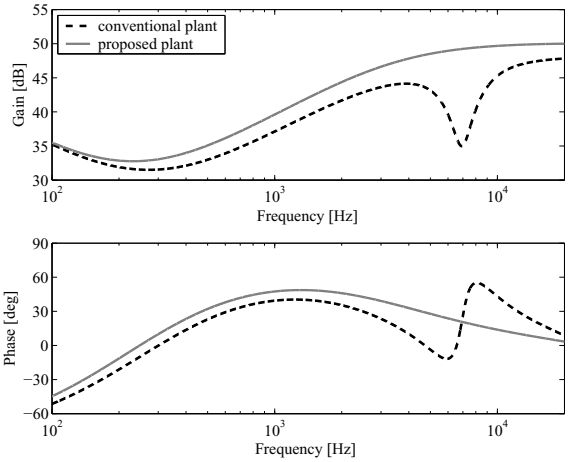

Fig. 9. Frequency characteristics of feedback compensator.

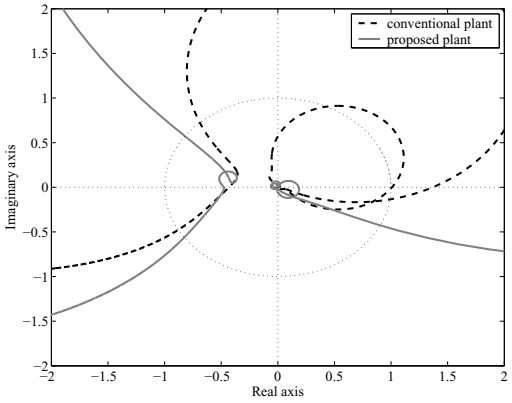

Fig. 10. Nyquist diagrams of positioning system.

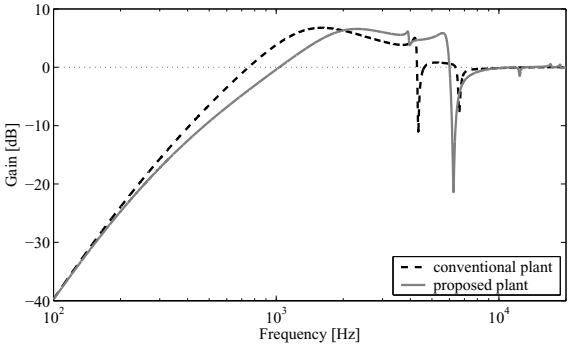

Fig. 11. Sensitivity characteristics of positioning system.

$C(z)$ in Fig.8 is a discrete implementation of $C_1(s)$ or $C_2(s)$ by a bilinear transformation with the sampling time T_s, while frequency characteristics indicate in Fig.9. Figs.10 and 11 show Nyquist diagrams and sensitivity characteristics for each control system, and Table IV lists the stability of control system. In these figures, dotted lines present the conventional plant without vibration node, while the solid lines present the proposed plant with vibration node. As the results of controller design, two vibration modes are compensated by phase-stabilization [11] using a notch filter in the conventional plant, while one vibration mode is compensated by only phase lead-lag filter in the proposed plant. In the proposed plant, therefore, since the notch filter can be removed for the feedback compensator, the order of $C(s)$ can be reduced. In addition, the expansion of servo bandwidth with the same stability shown in Table IV is achieved because the phase lag can be reduced. As a result, as shown in Fig.11, the reduction of sensitivity can be realized at around positioning frequency up to 1.3 kHz.

C. Design of feedforward compensator

In order to achieve the fast positioning and vibration suppression, the feedforward compensators $D(s)$, $N(s)$ are designed by the following coprime factorization of the plant model without the dead time component in (1) or (14).

$$P(s) = \frac{P_n(s)}{P_d(s)} = \frac{N(s)}{D(s)} \tag{17}$$
$$N(s) = P_n(s)F(s), D(s) = P_d(s)F(s)$$

$N(z), D(z)$ in Fig.8 are implemented in a discrete manner as the same procedure as of the feedback compensator. In this feedforward controller design, $D(s)$ generates the feedforward reference which cancels the plant resonant frequency, $N(s)$ generates the alternative position command trajectory r^*. The servo characteristic can be specified by a free parameter $F(s)$, independently of the feedback control performance. In this research, $F(s)$ is designed as a lowpass filter, where the parameters are designed to satisfy the same positioning time against both of plant, as well as to be proper $N(s)$ and $D(s)$. Fig.12 indicates gain characteristics of $N(s)$ and $D(s)$. From the figure, since it is not necessary to suppress the frequency component of primary vibration mode at around the servo bandwidth in the proposed plant, high frequency components in the control input u can be reduced. In addition, the order reduction of compensators can be also realized.

V. Experimental Verifications

The proposed approach is verified by experiments using the positioning device shown in Fig.2. Fig.13 shows the experimental results of positioning error $(r - y)$ of y for r, where the broken lines represent the conventional case of the plant without vibration node, and the solid lines represent the proposed case of the plant with vibration node. The upper waveforms in Fig.13 present the nominal plant condition

TABLE IV
STABILITY MARGIN OF POSITIONING SYSTEM.

	Gain margin	Phase margin	Gain crossover frequency
Conventional	7.7 [dB]	30 [deg]	1220 [Hz]
Proposed	6.4 [dB]	34 [deg]	1560 [Hz]

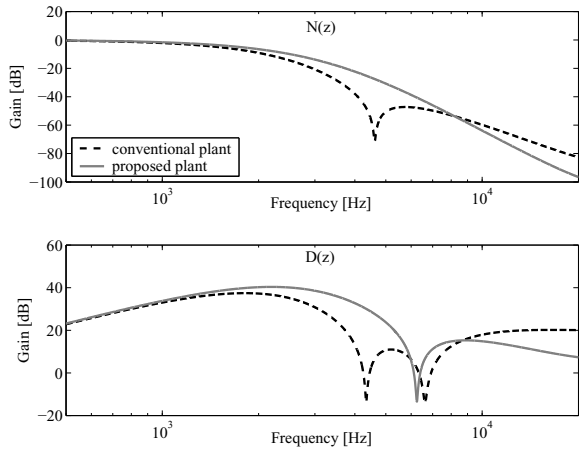

Fig. 12. Gain characteristics of feedforward compensator.

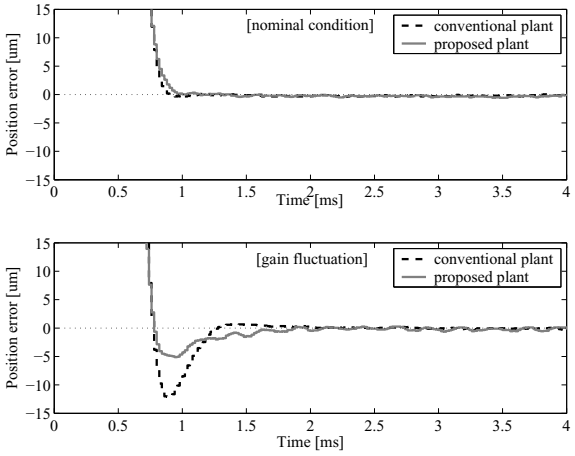

Fig. 13. Experimental waveforms of positioning error.

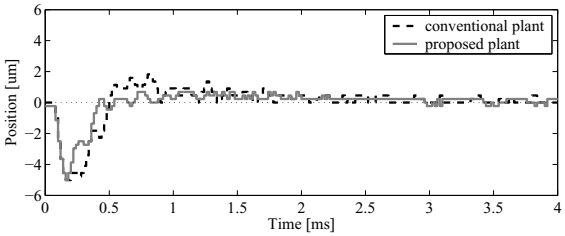

Fig. 14. Position responses for impulse disturbance.

without modeling error, while the bottom waveforms present the variation in torque constant. In this case, the gain reduction (2% for nominal value) is simulated by the temperature change of plant. From these results, in the nominal condition, the proposed plant shows the same performance as of the conventional plant without a notch filter. In the case of gain variation, on the other hand, the generation of overshoot can be reduced 60% by the proposed plant, because the servo bandwidth can be expanded and the sensitivity characteristic at around the positioning frequency can be improved. Fig.14 shows the experimental results for the disturbance of impulse force. From this result, the response converges to zero quickly without residual vibration by the expansion of servo bandwidth by the proposed plant.

VI. CONCLUSIONS

This paper presented a structural and controller design approach for the high-precision positioning for the galvano scanner with mechanical vibration modes, where the structural design using vibration node was proposed to cancel the primary vibration mode. In the structural design, the dynamic model of the plant was modeled by a lumped parameter model. Based on the model, the guideline of structural change was presented by the eigenvalue vector calculated by modal analysis. As a result, cancellation of the primary vibration mode was realized by simple structural change. By the design of positioning system for the proposed plant, the order reduction of compensators and the expansion of servo bandwidth could be realized. The effectiveness of the proposed approach has been verified by experiments using a positioning device for galvano scanners.

REFERENCES

[1] M. Tomizuka, "Advanced Control Applications to Servo Systems for Precision Machines", *Int. Conf. on MIPE*, pp.469–474, 1997.

[2] M. Hirata, T. Atsumi, A. Murase and K. Nonami, "Following Control of a Hard Disk Drive by using Sampled-Data H_∞ Control", *Proc. of the 1999 IEEE International Conference on Control Applications*, pp.182–186, 1999.

[3] M. Kobayashi, S. Nakagawa and S. Nakamura, "A phase-stabilized servo controller for dual-stage actuators in hard disk drives", *IEEE Trans. on Magnetics*, Vol.39, No.2, pp.844–850, 2003.

[4] F. Huang, T. Semba, W. Imaino and F. Lee, "Active Damping in HDD Actuator", *IEEE Trans. on Magnetics*, Vol.37, No.2, pp.847–849, 2001.

[5] S. Nakagawa, M. Kobayashi and T. Yamaguchi, "A Higher Bandwidth Servo Design with Strain Feedback Control for Magnetic Disk Drives", *Proc. of the American Control Conference*, pp.2547–2552, 2003.

[6] K. Seki, K. Mochizuki, M. Iwasaki and H. Hirai: "High-Precision Positioning Considering Suppression of Resonant Vibration Modes by Strain Feedback", *Proc. of the 35th Annual Conference of the IEEE Industrial Electronics Society*, pp.3114–3119 (2009)

[7] M. F. Chen and Y. P. Chen, "Compensating technique of field-distorting error for the CO_2 laser galvanometric scanning drilling machines", *Int. Journal of Machine Tools & Manufacture*, Vol.47, No.7-8, pp.1114–1124, 2007.

[8] N. Hirose, M. Iwasaki, M. Kawafuku and H. Hirai, "Initial Value Compensation Using Additional Input for Semi-Closed Control Systems", *IEEE Trans. on Industrial Electronics*, Vol.56, No.3, pp.635–641, 2009.

[9] I. Kajiwara, A. Nagamatsu, "Optimum Design of Optical Pick-Up by Elimination of Resonance Peaks", *Trans. of ASME, Journal of Vibration and Acoustics*, Vol.115, pp.377–383, 1993.

[10] I. Kajiwara, K. Tsujioka, A. Nagamatsu, "Approach for Simultaneous Optimization of a Structure and Control System", *AIAA Journal*, Vol.32, No.4, pp.866–873, 1994.

[11] M. Kobayashi, S. Nakagawa and S. Nakamura, "A phase-stabilized servo controller for dual-stage actuators in hard disk drives", *IEEE Trans. on Magnetics*, Vol.39, No.2, pp.844–850, 2003.